



OATAO is an open access repository that collects the work of Toulouse researchers and makes it freely available over the web where possible

This is an author's version published in: <http://oatao.univ-toulouse.fr/28842>

**Official URL:**

<https://doi.org/10.1177/13506501211040599>

**To cite this version:**

Jlail, Khoulood<sup>ORCID</sup> and Yahiaoui, Malik<sup>ORCID</sup> and Paris, Jean-Yves<sup>ORCID</sup> and Denape, Jean<sup>ORCID</sup> *Acoustic signature identification of damage and wear mechanisms in a steel/glass sliding contact.* (2021) In: Balkantrib 2020, 20 May 2021 - 22 May 2021 (Belgrade, Serbia).

Any correspondence concerning this service should be sent to the repository administrator: [tech-oatao@listes-diff.inp-toulouse.fr](mailto:tech-oatao@listes-diff.inp-toulouse.fr)

# Acoustic signature identification of damage and wear mechanisms in a steel/glass sliding contact

Khouloud Jlaiel , Malik Yahiaoui, Jean-Yves Paris and Jean Denape

## Abstract

The tribological behavior of a steel/glass ball-on-flat contact was studied by synchronizing the friction measurements with an acoustic emission device and a vision system. The results highlight two distinct friction regimes identified with low and high friction values. Their transition is characterized by a modification of acoustic emission signals. In addition, two main damage and wear mechanisms are identified: the creation and propagation of Hertzian cracks visible on the glass surface and the constitution of an interfacial layer of debris. The different accommodation mechanisms, activated successively or simultaneously, are identified for acoustic emission frequencies between 300 and 700 kHz. Eventually, this approach allows a real-time wear mechanisms identification and gives better insights about acoustic emission signals in relation to tribological systems.

## Keywords

Reciprocating sliding, acoustic emission, real-time observation, Hertzian cracks, third body, accommodation mechanisms

## Introduction

During friction, various tribological mechanisms can occur simultaneously and it is essential to better understand the evolution of these mechanisms from the contact setting to the establishment of a tribofilm, transfer film, and/or debris particles. In the common case of non-transparent frictional surfaces, this is a challenge due to the inaccessibility of the contact area during testing. The first bodies *post mortem* analysis gives information only on the final state of the contact area after multiple wear mechanism changes.

Over the last few decades, research has adopted several approaches to observe tribological processes. In situ techniques have been used to observe sliding dynamics, identify mechanical and/or chemical changes near the surface, and better understand the behavior of the third body for dry as well as lubricated contacts using optical microscopy, Raman spectroscopy, and camera observation.<sup>1-5</sup>

The acoustic emission (AE) technique, defined as the creation of transient elastic waves generated by local micro-displacements within a material,<sup>6</sup> can be utilized to reveal and monitor the tribological processes involved. In other words, it consists of measuring the elastic wave signal that is released by various sources in materials under stress (e.g. fracture, plastic deformation, and plowing). The underlying premise is that each elementary contact mechanism has a specific AE signature, which

could be characterized in terms of released energy and frequency.

In the literature, the AE technique has shown its sensitivity to detect unusual changes in friction systems. For example, Hase et al.<sup>7</sup> showed that AE signals are better suited for the identification of the different wear phenomena observed on worn steel surfaces. The AE signals are affected when there is a change in the wear mode and type of wear particles caused by variations in the sliding velocity. Moreover, the same authors found that a continuous AE signal of low amplitude is detected by the generation of slip lines in the frictional interface and by the generation and transfer of wear particles.<sup>8</sup> Meriaux et al.<sup>9</sup> identified three successive stages in the global crack propagation process in a fretting fatigue test. They demonstrate that short and inclined cracks initiate and propagate first due to the shearing process (mode II). Thus, AE cumulative activity increases gradually. Second, cracks propagate in a mixed mode of shearing

Laboratoire Génie de Production LGP, Université de Toulouse, INP-ENIT, 65016 Tarbes, France

### Corresponding author:

Khouloud Jlaiel, Laboratoire Génie de Production LGP, Université de Toulouse, INP-ENIT, 65016 Tarbes, France.

Email: [kjlaiel@enit.fr](mailto:kjlaiel@enit.fr)

and tension where the AE cumulative activity stabilizes. Finally, fatigue cracks propagate by tension in a pure mode I process where the AE cumulative activity reaches its maximum value. Similarly, Rastegaev et al.<sup>10</sup> explained that an increasing severity of wear is accompanied by a concomitant increase in the AE energy, which occurs in parallel with the decrease in the median frequency of the AE power-spectral density. Recently, Haas et al.<sup>11</sup> identified distinctive AE frequency ranges in plowing and cutting events. Also, Jlaiel et al.<sup>12</sup> observed a change in the AE signals associated with low friction, Hertzian cracks formation, and third body formation. Regarding the frequency band, a correlation map for the AE frequency band of several tribological phenomena has been established by Hase et al.<sup>13</sup> based on a literature review. This map allocates frequency bands and amplitudes to various interfacial accommodation modes and sources and even operating conditions. For instance, abrasive wear is identified between 0.2 and 1 MHz. On the same map, the authors represent a sliding friction frequency band under 200 kHz and a crack propagation one between 100 and 700 kHz. More surprisingly, large frequency bands related to fatigue and tensile testing are observed on the map at 600 kHz. These large frequency bands obviously enclose several elementary accommodation mechanisms of the tribosystem which are difficult to distinguish during the test and in *post mortem* analysis of the worn surfaces.

Eventually, most of the past studies propose correlations between AE signals and interfacial mechanisms without a direct and synchronous observation of these mechanisms. The main goal of this study is then to clearly correlate the AE signatures of the elementary wear damage and the accommodation mechanisms occurring within the contact using a real-time observation of the contact area between a steel ball and glass flat.

## Materials and methods

The Tribolumen tribometer used in this study allows simulating the fretting phenomena and reciprocating sliding close to fretting conditions on transparent materials.<sup>12</sup> This apparatus ensures the contact between a soda-lime glass sample and a 100Cr6 steel ball (AISI 52100, 6 mm in diameter,  $0.015 \pm 0.005 \mu\text{m}$  of average roughness) in a ball-on-flat configuration. The dry friction test was carried out under pure sliding conditions with an imposed stroke of  $100 \mu\text{m}$  (i.e. an amplitude of  $\pm 50 \mu\text{m}$ ), an excitation frequency of 10 Hz, and a normal load of 5 N, which correspond to a maximum contact pressure around 700 MPa (according to Hertz' theory). The maximum velocity relative to the glass sample displacement is around 9.36 mm/s. A high-speed camera is positioned on the soda-lime glass sample side. The camera is used at a frame rate of 500 fps to observe the contact area in real-time testing. The AE acquisitions were performed using two piezoelectric sensors fixed close to the contact. The sensors were set using a water-based adhesive containing a styrene acrylic copolymer. This adhesive

allows a good transmission of acoustic signals and dries in a few seconds and the sensors are easily detached after the experiments. The sensors (Micro-80 sensor from Mistras) have a large frequency band with a maximum sensitivity between 100 and 1000 kHz. The coupling of the sensors was then controlled by the Hsu–Nielsen source method described by the standard NF EN 1330-9. A threshold value of 27 dB was chosen to get finer detection without being disturbed by environmental conditions. The device synchronizes AE signals with friction data acquired by the tribometer. Before testing, the samples were cleaned for 15 min using an industrial detergent, then rinsed with demineralized water, and finally ultrasonically cleaned with ethanol for 10 min before being dried in an oven at 60 °C for 15 min.

The measurements of displacement and tangential and actuator forces were acquired using an HBM Quantum X system. In parallel, the measured acoustic signals that include various characteristic parameters to be considered were analyzed. They were directly processed using Mistras NOESIS™ software. The contact area image sequences were obtained through a high-speed camera and were analyzed using the ImageJ software. All the experiments were repeated three times and similar results were obtained.

## Results and discussions

### Frictional results

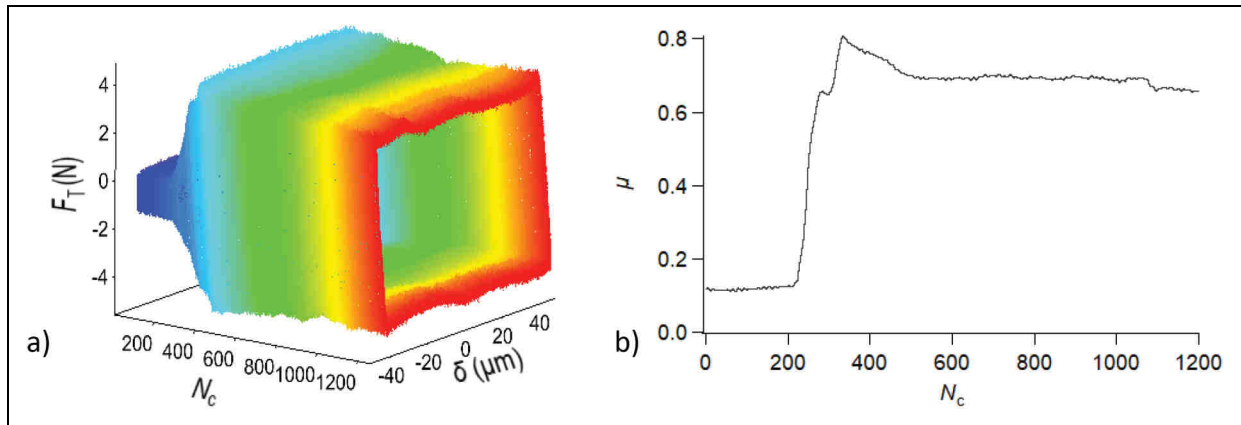
The experiments display classical fretting logs (Figure 1(a)). As the displacement is imposed, the fretting logs display a quasi-square section shape. The friction is relatively low at the beginning of a test and increases after 200 cycles to reach a steady value until the end.

Figure 1(b) presents the coefficient of friction  $\mu$  as a function of the cycle number. At the very beginning, the coefficient of friction is around 0.12. After about 200 cycles, this value increases abruptly to reach 0.8. Finally, after 420 cycles, the coefficient of friction stabilizes around 0.68.

### Wear results

The worn surfaces of the soda-lime glass and the 100Cr6 steel ball surfaces were observed systematically by optical microscopy without cleaning after 1200 cycles (Figure 2). The wear scar on the flat glass sample shows an expected elliptical shape with the smallest axis corresponding to the diameter of the wear scar on the steel ball (around  $178 \pm 1 \mu\text{m}$ ) and the largest axis oriented in the sliding direction. The central zones of the two worn surfaces have abrasion scratches. In the third body approach, this zone corresponds to the interface generating debris associated with the source flow and the internal flow. Debris is preferentially agglomerated on the soda-lime glass and ejected outside of the contact area, in the displacement direction, representing the wear flow.

Figure 3 shows a typical scanning electron microscopy observation of the third body after separating the



**Figure 1.** (a) Fretting log: tangential force versus number of cycles and (b) coefficient of friction sliding average for soda-lime glass against 100Cr6 ball steel ( $F_N = 5$  N,  $\delta = \pm 50$   $\mu\text{m}$ ,  $f = 10$  Hz).

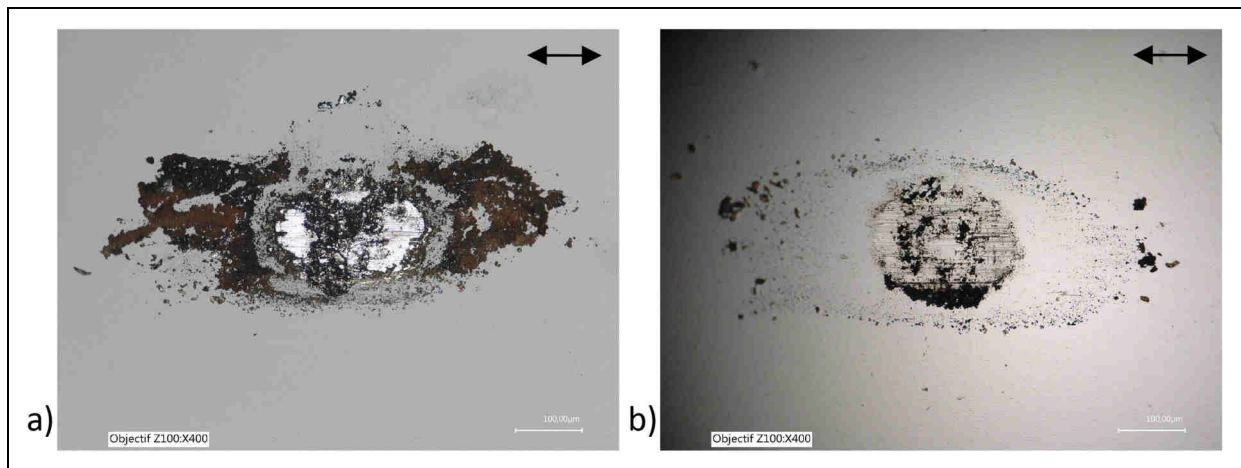


**Figure 2.** Optical microscopy of worn surfaces of (a) soda-lime glass and (b) 100Cr6 steel ball after 1200 cycles ( $F_N = 5$  N,  $\delta = \pm 50$   $\mu\text{m}$ ,  $f = 10$  Hz).  $\leftrightarrow$  Sliding direction.

ball and the flat. It is noted that debris is compacted together and adheres to the surface of the soda-lime glass sample to form an adherent interfacial layer. When the contact is opened and the ball is removed, the breakdown of this interfacial layer inevitably occurs as a result of the separation of tensile stress following the end of the tribological test (Figure 3(a)). Outside the wear track, ejected debris is found in fine particles with a diameter of  $1 \pm 0.5$   $\mu\text{m}$  and much larger particles with an average diameter of  $8.5 \pm 0.5$   $\mu\text{m}$  (Figure 3(b)).

The energy dispersive spectroscopy maps show that iron elements were transferred from the ball to the flat (Figure 4). These elements are more numerous in the central wear track than in the external wear track.

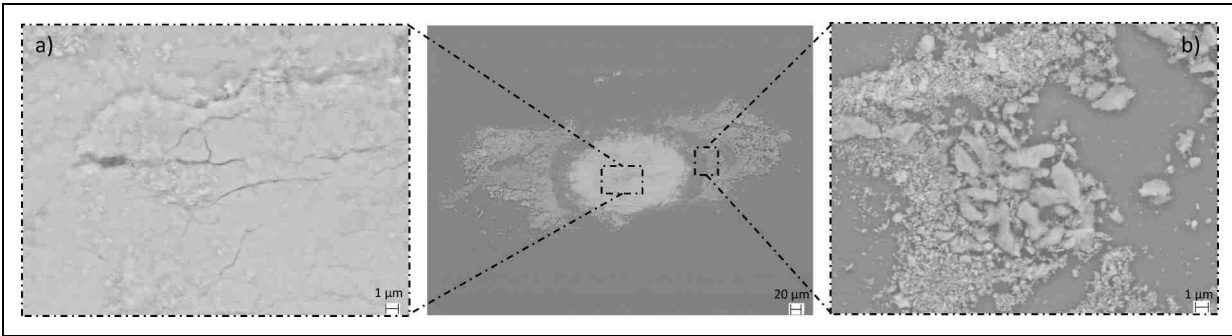
### AE results

Several characteristic parameters of AE signals were calculated and extracted from the recorded waveforms. For this study, only AE amplitude ( $A_{AE}$ ), absolute energy ( $E_{abs}$ ), and centroid frequency ( $f_c$ ) will be discussed as

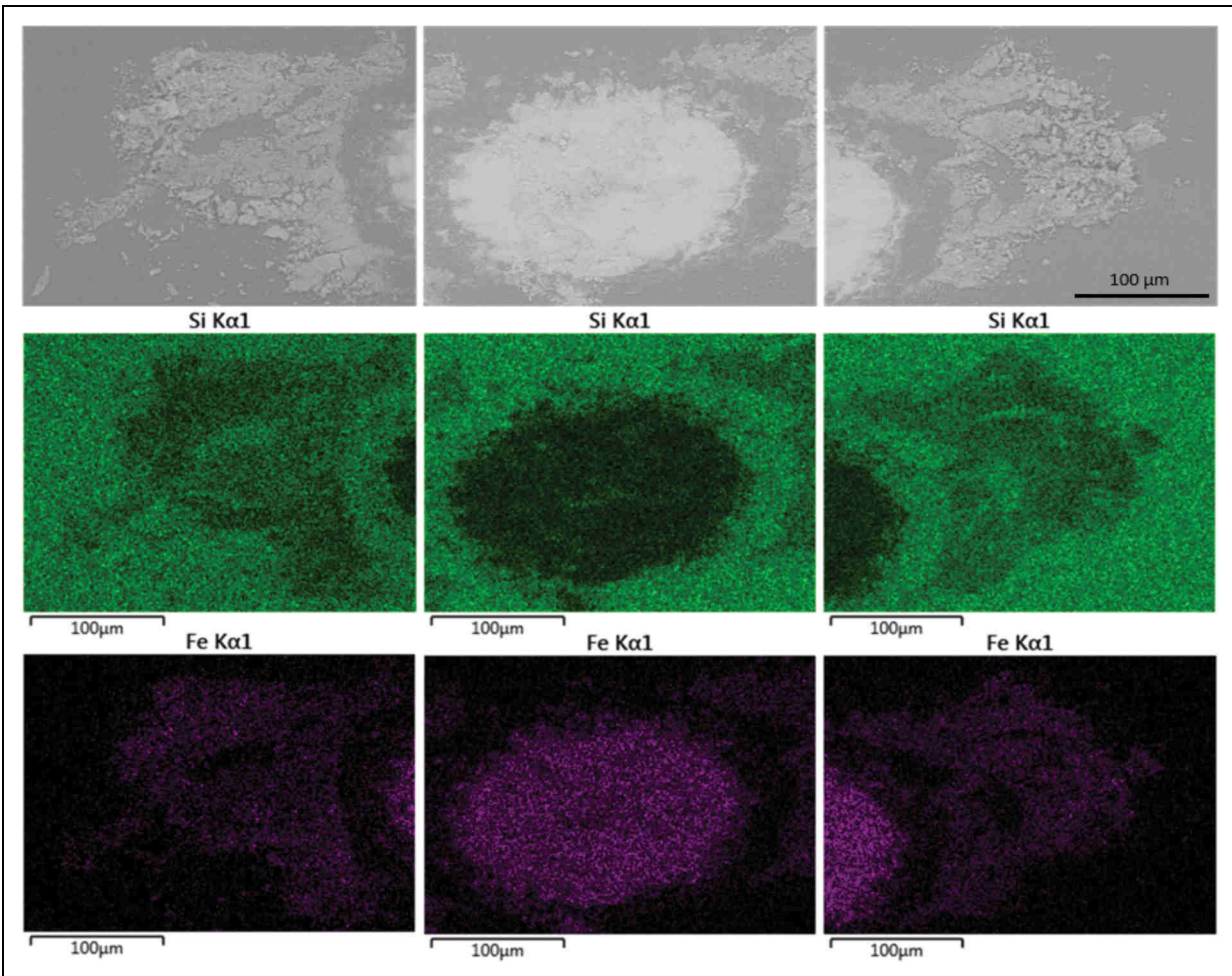
the most representative parameters. The AE amplitude represents the maximum amplitude of the signal during the test. The absolute energy represents the integral of the squared signal over the burst duration. The centroid frequency represents the frequency center of mass of the AE signals, that is, it characterizes the overall frequency content of an AE signal.

Figure 5 presents the variations of the amplitude, the centroid frequency, and the cumulative absolute energy during the friction test. Three distinct stages are identified synchronously with the evolution of the coefficient of friction:

- In the initial stage (until 200 cycles), the coefficient of friction was low and no AE signals were recorded over the experimental AE threshold detection level.
- In the intermediate stage, from 200 cycles until 420 cycles, the coefficient of friction increases abruptly. During this second phase, AE signals (hit) are recorded. They represent about 90% of the total AE energy emitted and are characterized by a wide range of frequencies (360–700 kHz) and amplitude (29–55 dB).



**Figure 3.** Scanning electron microscopy (SEM) observation of the third body (a) in the central wear track and (b) in the external wear track.



**Figure 4.** SEM observation and EDS analysis (Si and Fe) of the third body. SEM, scanning electron microscopy; EDS, energy dispersive spectroscopy.

- In the final stage (420 cycles to the end), the coefficient of friction is again relatively stable but high. During this third phase, the AE signals are low in energy (about 10% of the total AE energy emitted) and are characterized also by low amplitudes (29–35 dB), but high frequencies (500–700 kHz), compared with the second stage.

### *Correlation between tribological behavior and AE signals*

In this section, to better understand the phenomena occurring during the test, a representation of the coefficient of friction (Figure 6) is accompanied by images extracted from the video showing the evolution of damage

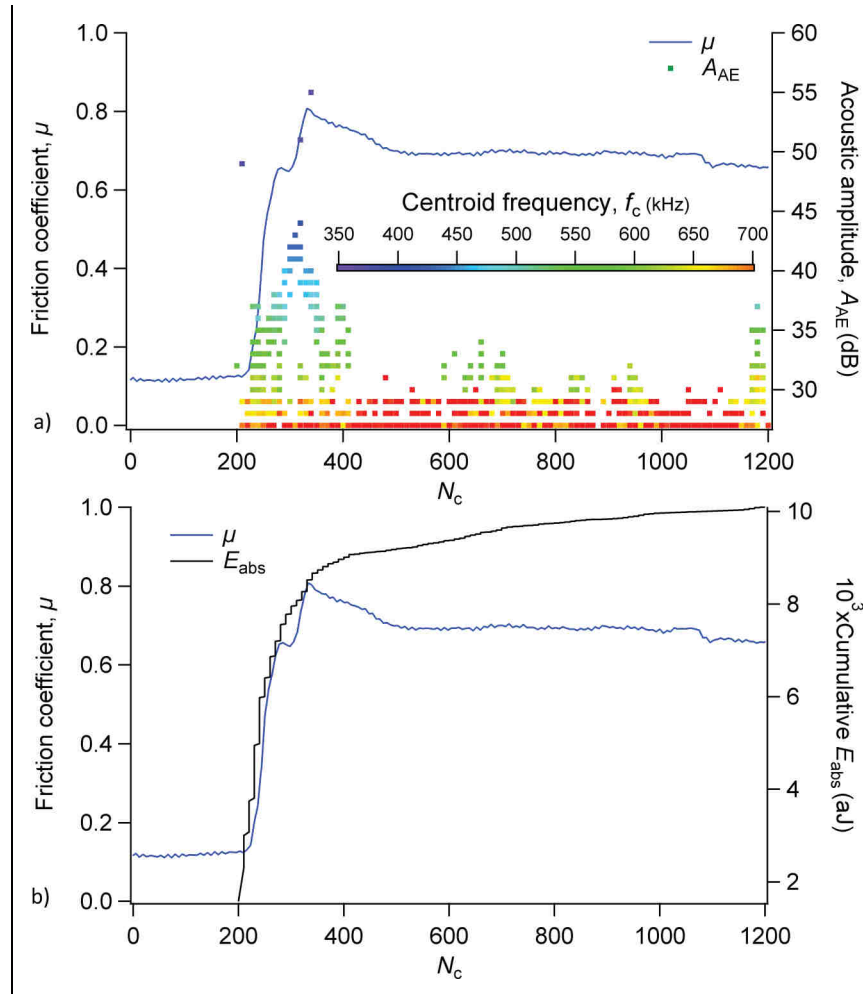


**Figure 5.** Evolution of (a) acoustic amplitude and (b) cumulative absolute energy during testing.

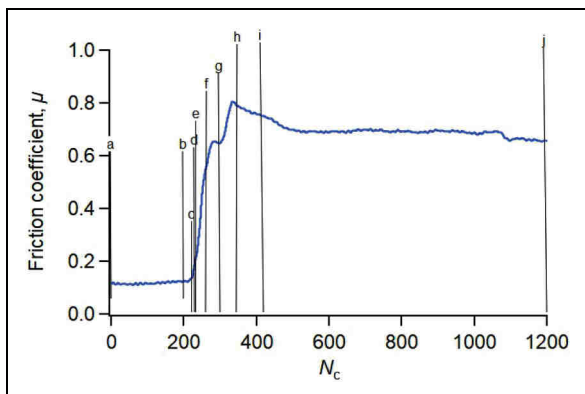
processes (Figure 7) at specific cycle numbers noted with letters from a to j.

Figure 7(a) shows the initial contact between the ball and the flat under a normal load of 5 N. The central, circular dark area is the contact area. Following Hertz's theory, the radius of this contact area is determined and is about 58  $\mu\text{m}$ , as can be observed. It is formed by elastic deformation. The white rings around this area

also called Newton's rings, corresponding to the optical interference fringes. They are caused by the divergence of the ball away from the glass sample surface.

In the first stage (until 200 cycles), the coefficient of friction remains very low (about 0.12) and no degradation in steel or glass surfaces is observed (Figure 7(b)). So, the accommodation has taken place by shearing in residual natural screens of the first bodies' surfaces. No AE signals were recorded over the experimental AE threshold.

After 200 cycles (beginning of the intermediate stage), natural screens have been destroyed by friction. Direct interactions between the surfaces of steel and glass samples occur, resulting in the creation/breakdown of adhesive junctions and therefore in a rise of coefficient of friction. This mechanism generates AE signals characterized by an acoustic amplitude close to 49 dB and a centroid frequency of 366 kHz. These results are similar to those observed by Kolubaev et al.<sup>14</sup> They show that when the real contact occurs between the conjugated surfaces and when the contact area increases, both the coefficient of friction and AE signal increase. The acoustic frequency reached in this case is around 340 kHz. Furthermore, as reported by Hase et al.,<sup>13</sup> the acoustic



**Figure 6.** The evolution of the coefficient of friction.

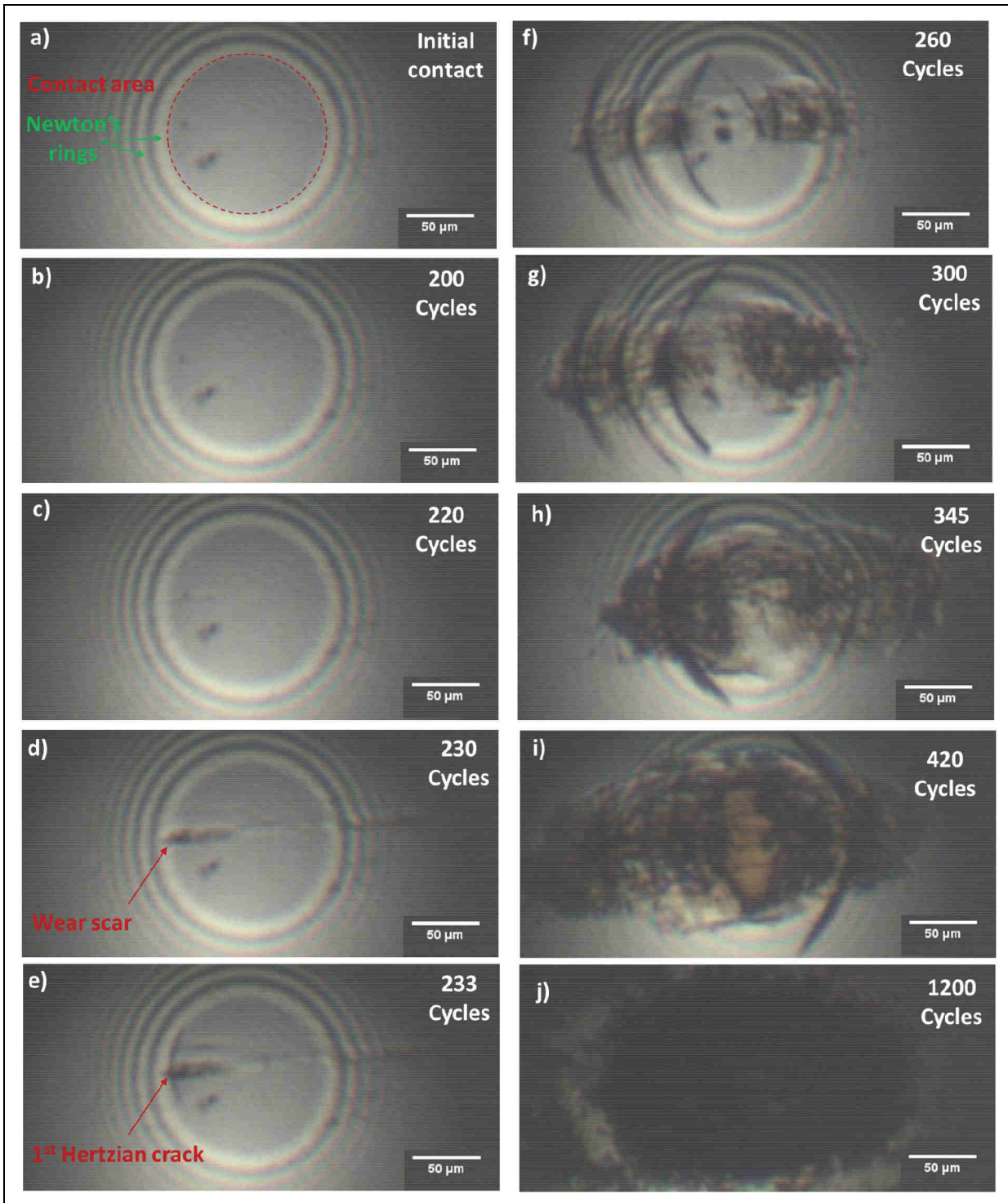


**Figure 7.** Images of the contact area extracted from the video showing the evolution of the damaging process during sliding friction. (a) and (b) in the first stage, from (c) to (h) in the intermediate stage, (i) and (j) in the final stage.

frequency band of the sliding friction and the breakage of the asperities are produced at a frequency band between 0.05 and 0.35 MHz.

At 220 cycles (Figure 7(c)), after multiple passes, particles are detached from the contact zones of the steel ball. They are transferred to the glass surface by adhesion and generate the source flow  $Q_s$ . These particles are trapped and circulated within the contact zone to initiate the

internal flow  $Q_i$ . A wear scar starts to form in the sliding interface and emits an acoustic amplitude close to 35 dB. Also, the wear scar evolves in terms of length (Figure 7(d)). These observations are in agreement with several studies, which have shown that the AE signals are sensitive to wear debris generation. Gen et al. showed that the AE energy could demonstrate the generation of wear debris, which emits a high-level signal.

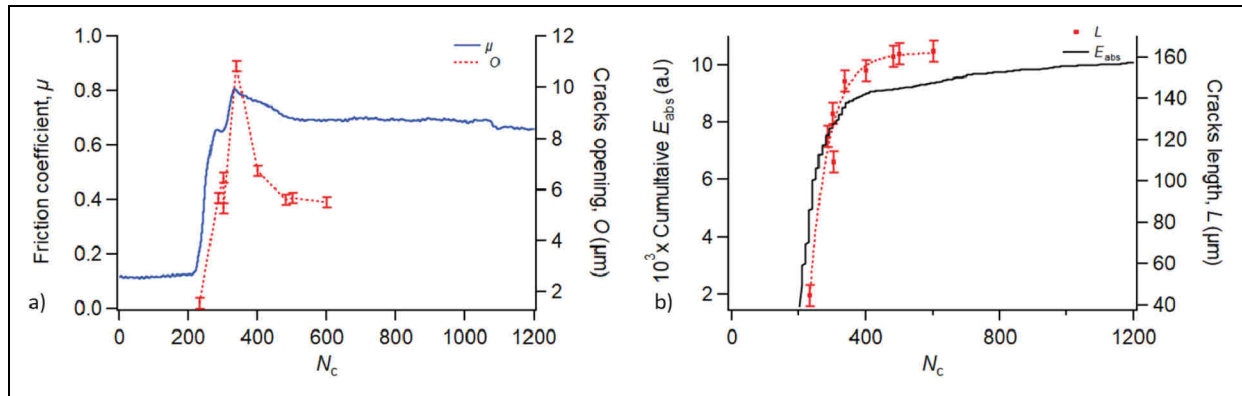


**Figure 8.** (a) Synchronized evolution of the coefficient of friction and crack opening during the test and (b) synchronized evolution of cumulative energy and crack length during testing.

Moreover, according to Sun et al.,<sup>15</sup> as soon as the sliding contact is effective, a lot of debris can easily be generated which leads to an increase of the AE signals.

At 233 cycles, a first Hertzian crack is observed on the glass sample (Figure 7(e)). The crack has a semicircular shape in which the concave side indicates the sliding direction when it occurred. This type of crack is usually observed on brittle materials such as glasses and ceramics. It originates from the stress distribution in the flat sample, which is induced by the ball displacement. For a sliding ball-on-flat contact, tensile stress appears behind the contact and leads to a fracture. In this stage, the centroid frequency is around 501 kHz. However, the AE amplitude increases to 37 dB, because the strain energy released by cracking is higher than that released by the formation of wear debris.

When the ball moves, the number of cracks increases. Figure 7(f) shows a series of three consecutive cracks at the back of the contact. In addition, with the reciprocal sliding of the ball, cracks can also appear completely or partially in the opposite sliding direction. The cracks are equally spaced (around  $36 \pm 1 \mu\text{m}$ ). This inter-crack spacing is generally related to the coefficient of friction and the fracture toughness of the glass.<sup>16,17</sup> Friction also produces compressive stress in the front of the sliding surface that closes the cracks generated during the previous part of the cycle when the displacement followed the opposite direction, so they are not more visible on the video. Such cracks are visible again when they are re-opened by tension behind the contact when the sliding is once more in the appropriate direction.

Figure 7(g) shows that detached particles continue to progress in terms of width. Their accumulation produces an adherent interfacial bed of powder that reduces the first bodies' surface interactions. A part of the detached particles is also ejected outside the contact zone and creates the wear flow  $Q_w$ .

At 345 cycles (Figure 7(h)), the abrupt increase of the coefficient of friction up to 0.8 is accompanied by the increase of the AE amplitude to 55 dB. This is due to the appearance of the largest Hertzian crack on the glass surface. In this intermediate stage of testing, cracks

length and opening are measured from the in situ observation. The maximum value of the crack opening reaches  $10.8 \pm 0.2 \mu\text{m}$  and follows the coefficient of friction evolution (Figure 8(a)). In contrast, the crack length increases monotonously from 44 to  $155 \pm 5 \mu\text{m}$  and follows the evolution of the acoustic cumulative  $E_{\text{abs}}$  (Figure 8(b)).

The detection of crack initiation and propagation during sliding contact has been investigated by Cadario and Alfredsson<sup>18</sup> They showed that an increase in acoustic events and a variation of the AE signal slope are related to crack growth. Moreover, Ramadan et al.<sup>19</sup> studied the AE originating from crack initiation and propagation. The frequency band associated with these phenomena is from 0.05 to 0.7 MHz. The AE amplitude attributed to the crack initiation was in the range between 23 and 30 dB. After that, the AE amplitude that is between 30 and 40 dB is associated with crack growth. The AE amplitude that is  $>55$  dB is associated with material failure. All these results are close to the results presented above.

In the final stage, starting at 420 cycles (Figure 7(i) and (j)), the coefficient of friction starts to stabilize at 0.68. The adherent interfacial layer continues to grow until it becomes extended to the entire contact area. Newton's rings and also cracks are no more visible. The AE signals are low compared to the second stage. This is similar to Ito et al.<sup>20</sup> results. They showed that in a steady-state stage the accumulation of wear debris between the contacting surfaces leads to relatively low values of AE signals despite a high coefficient of friction.

The shearing accommodation in this layer corresponds to a centroid frequency around  $650 \pm 1$  kHz. In the same way, the crack sizes (length and opening) start to stabilize, respectively, around  $160 \pm 5$  and  $6 \pm 0.2 \mu\text{m}$ . The accommodation mechanism is then made by crack opening/closing characterized by a centroid frequency at around  $550 \pm 1$  kHz.

## Conclusions

Ball-on-flat dry friction behavior of soda-lime glass against 100Cr6 steel was studied using an AE technique associated with direct observation by video through the contact. The study highlights the importance of



synchronizing friction measurements with real-time observation and AE signals continuously recorded during friction testing. The AE technique shows high sensitivity to tribological phenomena and has made it possible to detect several sources of AE generated during testing. These sources can be associated with damage or wear mechanisms: crack initiation and propagation, creation/breakdown of adhesive junctions (particle detachment), and shear accommodation mechanism in the interfacial layer. This approach allows a real-time wear mechanism identification and gives better insights into the AE signals in correlation with the tribological system.

The results show that:

- The accommodation mechanisms taking place by shearing in natural screens of the first bodies do not create AE signals over the experimental threshold.
- The direct interactions between the first bodies' surfaces (creation/breakdown of adhesive junctions) produce AE signals with a centroid frequency around  $366 \pm 1$  kHz.
- The initiation of the first Hertzian cracks is characterized by a centroid frequency around  $501 \pm 1$  kHz.
- In the stabilization period, the accommodation mechanism takes place by shearing in the interfacial layer at a centroid frequency around  $650 \pm 1$  kHz.
- In the stabilization period, the accommodation mechanism also takes place by cracks opening and closing at a centroid frequency around  $550 \pm 1$  kHz.
- Regarding crack sizes, the largest crack is characterized by the highest AE features.
- The crack opening follows the coefficient of friction evolution.
- The crack length follows the acoustic cumulative  $E_{abs}$ .


### Declaration of Conflicting Interests

The authors declared no potential conflicts of interest with respect to the research, authorship, and/or publication of this article.

### Funding

The authors received no financial support for the research, authorship, and/or publication of this article.

### ORCID iD

Khouloud Jlaiel  <https://orcid.org/0000-0003-3136-730X>

### References

1. Yahiaoui M, Rigaud E, Mazuyer D, et al. Forced oscillations dynamic tribometer with real-time insights of lubricated interfaces. *Rev Sci Instrum* 2017; 88: 035101.
2. Sriraman KR, et al. Tribological behavior of electrodeposited Zn, Zn–Ni, Cd and Cd–Ti coatings on low carbon steel substrates. *Tribol Int* 2012; 56: 107–120.
3. Eguchi M, Shibamiya T and Yamamoto T. Measurement of real contact area and analysis of stick/slip region. *Tribol Int* 2009; 42: 1781–1791.
4. Dvorak S, Wahl KJ and Singer IL. In situ analysis of third body contributions to sliding friction of a Pb–Mo–S coating in dry and humid air. *Tribol Lett* 2007; 28: 263–274.
5. Teng J and Sato K. In situ observations of fretting wear behavior in PMMA/steel model. *Mater Des* 2004; 25: 471–478.
6. Standard B. Non-destructive testing--Terminology Part 9: Terms used in acoustic emission testing, *BS EN 1330-9*: 2000, 2000.
7. Hase A, Wada M and Mishina H. Acoustic emission signals and wear phenomena on severe-mild wear transition. *Tribol Online* 2008; 3: 298–303.
8. Hase A, Mishina H and Wada M. Acoustic emission in elementary processes of friction and wear: In-situ observation of friction surface and AE signals. *J Adv Mech Des Syst Manuf* 2009; 3: 333–344.
9. Meriaux J, Boinet M, Fouvry S, et al. Identification of fretting fatigue crack propagation mechanisms using acoustic emission. *Tribol Int* 2010; 43: 2166–2174.
10. Rastegaev IA, Merson DL, Danyuk AV, et al. Using acoustic emission signal categorization for reconstruction of wear development timeline in tribosystems: case studies and application examples. *Wear* 2018; 410–411: 83–92.
11. Haas M, El Syaad K, Cihak-Bayr U, et al. Examination of undisturbed acoustic emission generated by experimentally modelled two-body abrasive wear events. *Tribol Int* 2020; 141: 105912.
12. Jlaiel K, Yahiaoui M, Paris J-Y, et al. Tribolumen: A tribometer for a correlation between AE signals and observation of tribological process in real-time-application to a dry steel/glass reciprocating sliding contact. *Lubricants* 2020; 8: 47.
13. Hase A, Mishina H and Wada M. Correlation between features of acoustic emission signals and mechanical wear mechanisms. *Wear* 2012; 292–293: 144–150.
14. Kolubaev EA, Kolubaev AV and Sizova OV. Analysis of acoustic emission during sliding friction of manganese steel. *Tech Phys Lett* 2010; 36: 762–765.
15. Sun J, Wood RJK, Wang L, et al. Wear monitoring of bearing steel using electrostatic and acoustic emission techniques. *Wear* 2005; 259: 1482–1489.
16. Hills DA, Munisamy RL, Nowell D, et al. Brittle fracture from a sliding Hertzian contact. *Proc. IMechE, Part C: J. Mechanical Engineering Science* 1994; 208: 409–415.
17. Geng X, Zhang Z, Barthel E, et al. Mechanical behavior of stiff coating on glass under sliding contact. *Wear* 2010; 269: 351–361.
18. Cadario A and Alfredsson B. Fretting fatigue crack growth for a spherical indenter with constant and cyclic bulk load. *Eng Fract Mech* 2005; 72: 1664–1690.
19. Ramadan S, Gaillet L, Tessier C, et al. Detection of stress corrosion cracking of high-strength steel used in prestressed concrete structures by acoustic emission technique. *Appl Surf Sci* 2008; 254: 2255–2261.
20. Ito S, Shima M, Jibiki T, et al. The relationship between AE and dissipation energy for fretting wear. *Tribol Int* 2009; 42: 236–242.